Journal of Hydrology 561 (2018) 1048–1062

Contents lists available at ScienceDirect

Journal of Hydrology

journal homepage: www.elsevier.com/locate/jhydrol

Research papers

Response of a fractured bedrock aquifer to recharge from heavy rainfall events

S.Y. Rathay, D.M. Allen *, D. Kirste

Department of Earth Sciences, Simon Fraser University, 8888 University Drive, Burnaby, British Columbia, V5A 1S6, Canada

ARTICLE INFO

Article history:
Available online 23 July 2017
This manuscript was handled by Corrado Corradini, Editor-in-Chief, with the assistance of Brian D. Smerdon, Associate Editor

Keywords:
Groundwater recharge
Heavy rainfall
Fractured rock
Groundwater seepage
Thermal infrared imagery
Stable isotopes of water

ABSTRACT

Climate change is predicted to lead to an increased frequency of high intensity rainfall events. The impact on groundwater resources, particularly in areas of fractured bedrock aquifer systems, requires knowledge of how recharge is affected. In this study, the response of a fractured bedrock aquifer to heavy rainfall events is characterized. The study area is the Gulf Islands, a temperate region in British Columbia, Canada. Of the 14 provincial observation wells with hourly groundwater level data, only three showed pronounced responses to heavy rain events and were analyzed in detail. A detailed analysis at one well suggests rises in groundwater level were better correlated to all rain events than exclusively heavy rain during summer. The strength of the correlation decreased as the rainfall intensity increased. Solution of the Green-Ampt equation for rainfall events of varying magnitude indicated that an increase in rainfall intensity leads to more surface ponding and overland flow. Thus, the occurrence of more frequent heavy rain events in the future may result in lower net recharge. Thermal infrared images in seepage areas and the $\delta^{18}O$ and $\delta^{2}H$ composition for precipitation and seepage suggest rapid seepage responses to heavy rain events and rapid seepage dissipation rates. The overall rapid response of the fractured bedrock was advantageous for studying the response of the system to heavy rain events.

© 2017 Elsevier B.V. All rights reserved.

1. Introduction

Global climate change projections indicate that the proportion of infrequent, extreme (heavy) precipitation events is anticipated to increase in the 21st century (Pall et al., 2007; Owor et al., 2009; Intergovernmental Panel on Climate Change (IPCC), 2012; Taylor et al., 2013). The projected increase in heavy precipitation events will occur at a faster rate than mean precipitation, although projections vary by latitude (Allen and Ingram, 2002). The rainout of moisture by heavy precipitation events would deplete the atmosphere of moisture and reduce the occurrence of more frequent, lesser magnitude events (Pall et al., 2007; Owor et al., 2009).

It is uncertain, however, whether more heavy rainfall events will lead to an increase or decrease in groundwater recharge. Most studies on the impacts of climate change on recharge have focused on changes in total annual or monthly precipitation (e.g. Scibek and Allen, 2006; Jyrkama and Sykes, 2007; Toews and Allen, 2009). Furthermore, the few studies that have considered how shifts in the frequency and magnitude of events might influence aquifers have focused on either tropical regions or arid/semi-arid regions (Mileham et al., 2009; Owor et al., 2009; Taylor et al., 2013). Insufficient research has been carried out in temperate regions to understand how recharge responds to heavy rainfall events.

Groundwater recharge can be one of the most difficult components of a water balance to quantify and is often approximated or inferred by studying the response of the aquifer (Crosbie et al., 2010; Healy and Scanlon, 2010). The response of an aquifer to recharge is manifested, for example, in changes in groundwater level or changes in discharge. Such responses have been measured across a wide range of spatial and temporal scales, using a variety of methods (e.g., de Vries and Simmers, 2002; Scanlon et al., 2002; Healy and Scanlon, 2010).

Studies have shown that the amount and timing of precipitation play a key role in the overall aquifer response (Green et al., 2011). Of particular relevance to this study, rainfall rates during heavy rain events (herein considered high intensity rain events) may exceed the infiltration capacity of the subsurface, leading to ponding and infiltration excess overland flow (Dingman, 2002). Provided the water table remains below ground surface, infiltration (leading to recharge) will slow to a steady rate equal to the saturated hydraulic conductivity of the geological materials. Thus, higher precipitation rates will not necessarily correspond to increased recharge rates. In contrast, saturation excess overland

* Corresponding author.
E-mail address: dallen@sfu.ca (D.M. Allen).

http://dx.doi.org/10.1016/j.jhydrol.2017.07.042
0022-1694/© 2017 Elsevier B.V. All rights reserved.

flow occurs when the soil becomes saturated, and any additional rainfall that falls (irrespective of intensity) becomes overland flow. Therefore, the propensity of an area to produce runoff is largely independent of rainfall intensity. Rather, the total rainfall amount (intensity and duration) and landscape factors such as available water storage capacity in the geological materials, local topography, and recharge area, will influence whether or not a particular area will generate runoff.

The relation between rainfall and recharge has been previously demonstrated using linear regression analysis (Owor et al., 2009; Carretero and Kruse, 2012; Allocca et al., 2015; Turkeltaub et al., 2015). Turkeltaub et al. (2015) used a linear model to show that recharge was better related to annual precipitation from the previous year than the current year in a deep vadose zone sandy formation in a Mediterranean climate. Carretero and Kruse (2012) plotted monthly water table fluctuations against monthly precipitation during the wet and dry season, and demonstrated that less rainfall was necessary to create a rise in the water table during the dry season than the wet season. Allocca et al. (2015) used the Episodic Master Recession (EMR) method (Nimmo et al., 2015) to estimate the amount of recharge generated episodically by individual rainfall events and estimate the Recharge to Precipitation ratio (RPR) on a storm-by-storm basis. Finally, and of particular relevance to this study, Owor et al. (2009) investigated the impact of changing rainfall intensities on groundwater recharge in the Upper Nile Basin, Uganda (tropical climate). They found that the magnitude of groundwater recharge was better correlated to heavy rainfall events than all daily rainfall events.

In fractured rock, the factors that govern recharge are relatively poorly understood (Gleeson et al., 2009) and difficult to characterize due to preferential flow along fractures, resulting in non-uniform infiltration, and difficulties obtaining direct measurements of recharge (Gburek and Folmar, 1999; Healy and Cook, 2002; Scanlon et al., 2002; Heppner et al., 2007; Dvory et al., 2016). Previous studies have modeled infiltration to fractured bedrock with success (Katsuyama et al., 2005; Tromp-van Meerveld et al., 2007; Salve et al., 2008; Haught, 2010). Haught (2010) measured cumulative infiltration at three bedrock outcrops in a watershed in British Columbia, Canada and fit the observed data to three infiltration models: the Horton (1940), Philip (1957), and Green and Ampt (1911) models. Haught found that traditional infiltration models could be applied to fractured bedrock, although each model underestimated and overestimated infiltration at times. The model was generally insensitive to changes in model parameters. Salve et al. (2008) found that over long periods of time, such as prolonged flooding, infiltration rates to fractured bedrock demonstrated temporal anomalies and spatial variability. They attributed the temporal anomalies to phenomena such as clay swelling, erosion of loose filling debris, and entrapment of air. Although studies have examined the impact of bedrock infiltration on surface hydrology, to the knowledge of the authors, none appear to have examined how infiltration dynamics in bedrock change with differing rainfall intensities.

The high hydraulic conductivity and low storage capacity of fractures leads to rapid groundwater response rates (Kohut et al., 1984; Gburek and Folmar, 1999; Healy and Cook, 2002; Heppner et al., 2007). The potential for a rapid response in fractured bedrock aquifers makes them particularly well suited to studying how the aquifer responds on short time scales, for example, to individual heavy rain events. Moreover, the rapid flow of groundwater may manifest as the sudden appearance or increase in groundwater discharge in the form of springs, seeps, and baseflow to surface water bodies (de Vries and Simmers, 2002; Heppner et al., 2007). For this reason, examining the groundwater discharge environment may be useful for characterizing the aquifer response to heavy rainfall events.

Using heat as a tracer is one means to study groundwater processes in discharge environments (Anderson, 1995). In particular, infrared thermography has recently gained popularity due its relatively low cost, its non-destructive nature, and its ability to produce an instant, high-resolution image (Banks et al., 1996; Roeper et al., 2014). Popular applications of handheld and infrared technology examine discrete groundwater discharge (Deitchman and Loheide, 2009; Pandey et al., 2013; Vivas Becerra, 2014), surface water-groundwater interactions (Pfister et al., 2010; Schuetz and Weiler, 2011; Hare et al., 2015), and submarine groundwater discharge (Roeper et al., 2014).

This study aims to characterize the response of a fractured bedrock aquifer in a temperate region to heavy rainfall events. The research examines characteristics of both the recharge and discharge environments. Recharge, for the purpose of this study, refers to the vertical flow of water from infiltration of precipitation that reaches the water table and contributes to groundwater storage (Healy and Scanlon, 2010). For recharge characterization, a regression analysis is first carried out to correlate historical rainfall events to rises in groundwater level to determine a threshold rainfall amount that results in a distinguishable response in groundwater level. An analytical model is used to explore the relation between rainfall intensity and infiltration, and to estimate the impact of more frequent heavy rainfall events on groundwater recharge in the future. Field studies are carried out to investigate the discharge environment. Specifically, a FLIR thermal infrared camera is used to capture images of seepage during a rainfall event of high intensity. The FLIR imagery is used in combination with the stable isotope composition ($\delta^{18}O$ and $\delta^{2}H$) of seepage and precipitation to interpret rainfall-seepage processes. While numerous studies have used $\delta^{18}O$ and $\delta^{2}H$ to investigate recharge and discharge dynamics in fractured bedrock (e.g., Lee et al., 1999; Abbott et al., 2000; Gleeson et al., 2009; Praamsma et al., 2009), coupling stable isotope analysis with thermal infrared imagery offers a unique opportunity to conceptualize the rainfall-seepage process in response to a range of magnitude rainfall events. The Gulf Islands in British Columbia, Canada was selected as the study site due to the fractured nature of the bedrock, temperate climate, and fact that the majority of precipitation falls as rain (no snowmelt processes).

2. Material and methods

2.1. Study area

The Gulf Islands are comprised of two northern and eleven southern major islands in the Strait of Georgia between Vancouver Island and southwest mainland British Columbia (Fig. 1). One of the northernmost Gulf Islands, Gabriola Island, was the site of data collection to investigate the discharge environment (Fig. 2). Gabriola has an area of 57.73 km^2; it is approximately 14 km long and 4.2 km wide (Islands Trust, 2009; Statistics Canada, 2015). Elevation is highest near the center of the island at Stony Ridge (160 masl) and decreases shoreward with the steepest relief along the northern and southern coasts (Islands Trust, 2009). Land cover on the island consists predominantly of forest (~70% of the land area is tree covered – mostly Douglas fir), with the remainder as urban, agricultural and other. The understory of much of the forested areas of Gabriola Island consists of salal.

Climate on the Gulf Islands is temperate with mild, wet winters and cool, dry summers. The majority of precipitation falls as rain from October to April. On Gabriola, monthly precipitation normals over the period 1981 to 2010 ranged from 24.5 mm in July to 156.9 mm in November, with an average annual precipitation of 958 mm (data from Environment Canada, 2016). According to Environment

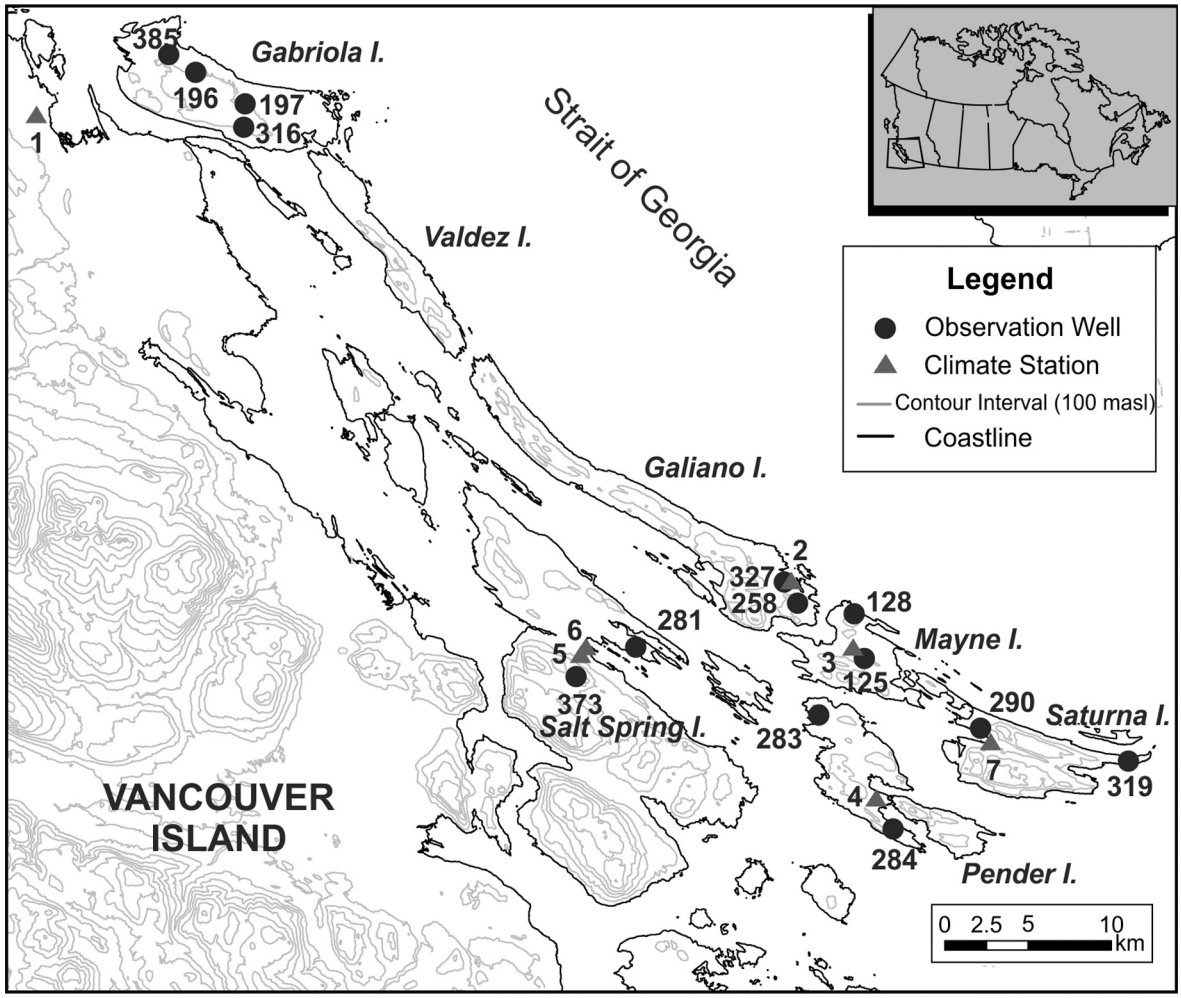

Fig. 1. The Gulf Islands in British Columbia, Canada. Map shows the location of provincial observation wells and selected climate stations.

Canada (2016), an average of 30.9 days per year experienced 10 mm or more of precipitation, and 4.5 days experienced 25 mm or more over the period 1981–2010. The majority of heavy rain events occurred during the winter.

The bedrock of the Gulf Islands belongs to the Late Cretaceous Nanaimo Group (~91–66 Ma), a group of marine sedimentary formations (Mustard, 1994) (Fig. 2). The formations alternate between coarse and fine-grained, mainly sandstone and conglomerate, and mudstone and fine-grained sandstone, respectively (Mustard, 1994). The four youngest formations of the Nanaimo Group (the Northumberland, Geoffrey, Spray, and Gabriola) are exposed on Gabriola Island (Fig. 2) England, 1989). Because the coarser-grained strata are more resistant to weathering than the finer-grained strata (Allen and Suchy, 2001), steep relief has formed along contacts where the less-resistant Northumberland and Spray Formations have eroded, leaving behind the Geoffrey and Gabriola Formations (Fig. 2). A layer of thin surficial deposits overlies the bedrock. These deposits are fluvial, marine, and glacial in origin, and reach a maximum of 7 m thick (Dakin et al., 1983).

The Nanaimo Group was considerably deformed through compression, uplift, erosion, and post-glacial isostatic rebound (Clague, 1986; Mustard, 1994). Structurally, the main feature on Gabriola is a syncline that runs northwest-southeast along the middle of the island, causing bedding to dip 10-15° toward the fold axis, and elevation to decrease shoreward (Fig. 2; England, 1989; Scibek et al., 2013). Three major faults (Gabriola Fault, Flat Top Islands Fault, and an unnamed fault) are also present on Gabriola (Fig. 2; Scibek et al., 2013). Secondary permeability increases the hydraulic conductivity variably according to structural setting and lithology (Surrette et al., 2008). In particular, bedding contacts, joints, and fracture zones serve as preferential pathways for fluid flow and aquifer recharge (Surrette and Allen, 2008). Based on the results of pumping tests and tidal response tests, the hydraulic conductivity ranges from 8.1×10^{-8} m/s to 1.5×10^{-6} m/s within the sandstone units and 2.4×10^{-7} m/s to 7.6×10^{-7} m/s within the mudstone units (Larocque, 2014). The mudstones are slightly more conductive due to the closer joint and bed spacing (Mackie, 2002).

Recharge modeling on Gabriola Island, using MIKE SHE (DHI, 2007) estimated the mean annual actual evapotranspiration to be in the range of 35–55% of mean annual precipitation, runoff of 29–42%, and recharge 17–26% (Burgess, 2017).

2.2. Groundwater level – rainfall regression analysis

Historical rainfall data were obtained from the School-Based Weather Station Network, a network consisting of 166 weather stations located on or nearby Vancouver Island (Weaver and Wiebe, 2012a, 2015). Rainfall was measured minute-by-minute using a tipping bucket rain gauge assembled in an open area far from any obstructions (Weaver and Wiebe, 2012b); the data were averaged hourly (Weaver and Wiebe, 2016). Snow was measured as rain once it melted, but should not contribute significantly to error due to the infrequency of snowfall

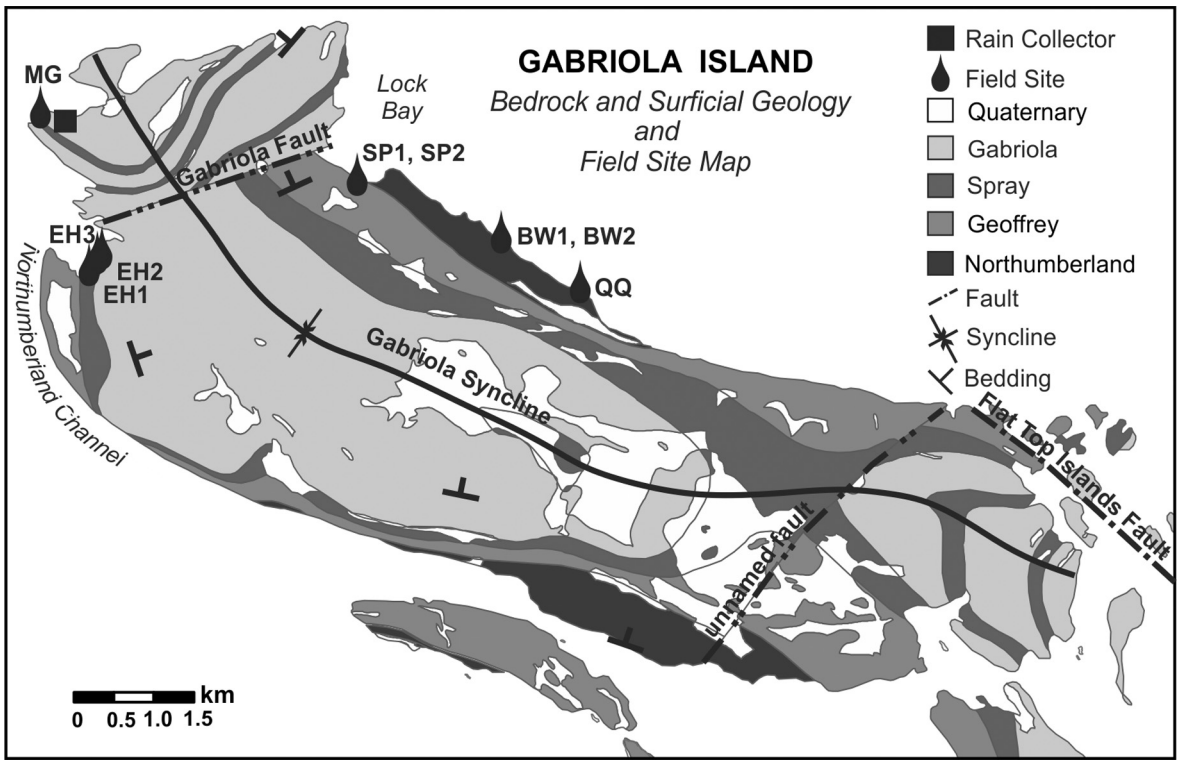

Fig. 2. The geology and data collection sites on Gabriola Island (geology from England, 1989; Natural Resources Canada). Sandstone dominated units (Gabriola and Geoffrey) are shown in lighter grey and mudstone dominated units (Spray and Northumberland) in darker grey. Bedding measurements are approximated from Mackie (2002).

(Weaver and Wiebe, n.d.). Overall, this network was chosen due to the frequency of measurements and proximity to provincial observation wells, which is critical due to the high temporal resolution of the data.

Groundwater levels on six Gulf Islands have been measured in provincial observation wells operated by the BC Ministry of Environment (2015) from as early as 1972. Records are available for download from the British Columbia Groundwater Observation Well Network website (BC Ministry of Environment, 2015). Historically, observation wells recorded groundwater levels at monthly intervals. But beginning in 2003, data collection increased to sub-daily (4 times per day) and soon after to hourly. For the purpose of this study, only those years that recorded hourly groundwater level measurements in all observation wells were considered (see Supplementary Information for hourly groundwater level and averaged hourly rainfall data, and corresponding hydrographs). Hourly data, which are not widely available in many areas, and therefore novel to this study, allowed for close examination of the groundwater response to shorter interval, high intensity rain events.

Hourly groundwater level data were extracted from 14 provincial observation wells over the period 2009–2015 (the high resolution period of record). Trends in groundwater level were first removed by differencing consecutive hourly values. Rainfall data from seven of the nearest School-Based Weather Stations, located 0.08–13 km from the wells (see Fig. 1) were extracted. Cross-correlation analysis was conducted to determine the correlation and lag time between rainfall amount and hourly fluctuations in groundwater level. Significant correlations were considered to be those exceeding the 95th percent confidence interval.

According to Cuthbert (2010), the timing and magnitude of the water table response may vary seasonally depending on antecedent conditions, evapotranspirative demand, hydraulic properties, and the depth to the water table. Thus, the response time of groundwater level to rainfall can be expected to vary by season. Cross-correlation analysis was also applied to determine the season with the highest correlation between rainfall and groundwater level fluctuations. The seasons were defined as autumn (September, October, November), winter (December, January, February), spring (March, April, May), and summer (June, July, August).

Regression analysis was conducted to determine if there is a threshold rainfall intensity that results in a distinguishable response in groundwater level, and what factors may influence this relationship. Analyses were performed during the season with the highest correlation, identified in the cross-correlation analysis. The relation between groundwater level rise and rainfall amount was based upon the water table fluctuation method, which assumes that variations in water level are a result of recharge arriving at the water table from precipitation. Regression analysis was carried out in RStudio (RStudio Team, 2015). The variables, rainfall amount and groundwater level rise, were fit to a linear regression model (e.g., Owor et al., 2009; Carretero and Kruse, 2012; Turkeltaub et al., 2015). The variance of the response variable and normality of the residuals were visually inspected to ensure that the data met the requirements for a regression analysis. The coefficient of determination, or R^2, was used to estimate how well the least squares regression line (LSRL) fit the data.

Data manipulation was performed to explore how to best represent the data, and subsequently, four regression analyses were carried out using groundwater level data and the nearest weather station:

1. Hourly groundwater level rise against hourly lagged rainfall amount. The lag time was estimated based on the peak lag time in a cross-correlation analysis where significant correlations were considered to be those exceeding the 95th percent confidence interval.
2. Hourly groundwater level rise against 24-h accumulated rainfall. Thus, the rain event was defined as rain that occurred within the last 24 h of each hourly rise in groundwater level.

3. Daily groundwater level rise against the same-day rainfall amount.
4. The magnitude of the groundwater level rise against the accumulated rainfall during a rain event, estimated manually. This method (referred henceforth as the manual method) related the magnitude of the groundwater level rise to a particular rain event if the rain preceded the change in groundwater level by approximately the estimated lag time from the cross-correlation analysis.

Once the best methods were identified, the relation between groundwater level rise and rainfall intensity was determined. For any well that showed a moderate to strong relationship between rainfall amount and groundwater level rise, rain was further classified as light or heavy rainfall intensity using a percentile-based approach. Rainfall above a light rain threshold (10th and 25th percentile, or 0.09 mm/hr and 0.17 mm/hr) or below a heavy rain threshold (50th, 75th, and 90th percentile; or 0.42 mm/hr, 0.87 mm/hr, and 1.25 mm/hr, respectively) was removed, and the remaining rainfall total was plotted against groundwater level rise for each individual rainfall intensity threshold.

2.3. Analytical modeling

An analytical model, based on a modified version of the Green and Ampt equation (Mein and Larson, 1973), was constructed to examine the rainfall-runoff-infiltration process in response to a range of magnitude rain events. The Green and Ampt equation (Green and Ampt, 1911) describes infiltration under a ponded surface assuming one-dimensional flow, homogeneous soil, a piston-like wetting front, and uniform antecedent moisture content (Chu, 1978; James et al., 1992; Mein and Larson, 1973). The equation can be written as:

$$f_p = K_s\left(1 + \frac{M_d * |S|}{F}\right) \quad (1)$$

where f_p is the infiltration capacity, K_s is the saturated hydraulic conductivity, M_d is the initial moisture deficit for the range $\theta_s - \theta_i$ (where θ_s is the saturated moisture content and θ_i is the initial moisture content), S is the capillary suction at the wetting front, and F is the cumulative infiltration since rainfall began (Mein and Larson, 1973).

Several studies have modified the Green and Ampt equation (Bouwer, 1969; Chu, 1978; Mein and Larson, 1973). In particular, Mein and Larson (1973) modified the Green and Ampt equation such that it is not limited to infiltration under a ponded surface. The equation determines the amount of infiltration prior to ponding and the time at which ponding begins, respectively:

$$F_s = \frac{|S_{av}| * M_d}{\frac{I}{K_s} - 1},\ I \geqslant K_s \quad (2)$$

$$t_p = \frac{F_s}{I} \quad (3)$$

where F_s is the cumulative infiltration prior to surface saturation when the rainfall intensity, I, is greater than or equal to K_s, S_{av} is the average capillary suction at the wetting front, and t_p is the time until surface ponding. Furthermore, Mein and Larson (1971) substituted dF/dt for f_p into Equation 1, separated the variables, and integrated to obtain an equation for cumulative infiltration as a function of time. The equation can be written as (Walter, 2011):

$$t = t_p + \frac{1}{K_s}[F - F_s + |S_{av}| * M_d * \ln\left(\frac{|S_{av}| * M_d + F_s}{|S_{av}| * M_d + F}\right)] \quad (4)$$

In this study, cumulative infiltration prior to surface ponding (Equation 2), the time of ponding (Equation 3), and infiltration rate (Equation 1) at numerous time intervals (Equation 4) for 10th, 25th, 50th, 75th, and 90th percentile rainfall events were modeled. However, when the rainfall intensity was less than the saturated hydraulic conductivity, the rainfall duration was assumed to be equivalent to the cumulative infiltration divided by rainfall intensity, and the infiltration rate was identical to the rainfall intensity. Rainfall percentiles were based upon historical hourly rainfall data measured at the Bayview Elementary School Weather Station, located 5.2 km west of Gabriola Island (Station 1 in Fig. 1; Weaver and Wiebe, 2016). A wide range of magnitude rain events was selected to illustrate the relationship between rainfall intensity and infiltration, as well as for consistency with the regression analysis.

In addition to rainfall intensity, the equations require values for saturated hydraulic conductivity, K_s, initial moisture content, θ_i, saturated moisture content, θ_s, and average capillary suction at the wetting front, S_{av}. Values for these parameters, representing the properties of the unweathered bedrock, can be found in Table 1. The bedrock was assumed to be exposed with no surficial deposits for simplification, and because the infiltration capacity of the bedrock is expected to be exceeded prior to the soil. The values for K_s and S_{av} were taken from Haught (2010) who measured cumulative infiltration at three fractured bedrock outcrops. Of the three outcrops, values were used for the largest outcrop (2.26 m^2), which was thought to best represent average fracture characteristics, therefore reducing the likelihood of discrete fractures influencing the hydraulic properties (Haught, 2010). The value of θ_s was derived from studies reporting porosity of the Nanaimo Group, the primary bedrock type on the Gulf Islands. Dakin et al. (1983) and England (1989) reported primary porosity to be <5%. Surrette et al. (2008) calculated porosity using a discrete fracture network approach. They found that potential porosity, representing the volume of fracture void space per unit volume of rock, ranged from 0.004 to 0.2% (mean value of 0.1%) for an assumed fracture aperture of 100 μm. The porosity in this study, and consequently θ_s, was taken to be a median value of 1%, or 0.01. Because the precise value for θ_i is unknown, a range of values, from 0.005 to 0.009 were considered to represent the range of potential initial moisture contents for the expected range of porosity.

2.4. Thermal infrared imagery

Gabriola Island was visited on four occasions in 2015 and 2016: June, September, November, and January. The timing of visits corresponded to dry conditions and a range of magnitude rainfall events. The Real-Time Ensemble Weather Forecast, WRF2 N model (36 km resolution), was used to predict the intensity, duration, and timing of upcoming rain events (UBC Earth, Ocean and Atmospheric Sciences, 2016).

Potential seeps were identified in the first several visits to Gabriola. These locations consisted of outcrops with visible fractures or bedding planes, often at the base of slopes. The outcrops frequently had visible seepage, or watermarks, indicating that seepage had occurred in the past. In total, eight potential seeps were identified (BW1, BW2, EH1, EH2, EH3, MG, SP1, and SP2) but only one seep (EH2) was selected to examine the seepage response to a heavy rainfall event in January 2016 (maximum rain intensity = 3.5 mm/h, rain total = 42.9 mm) (data from Weaver and Wiebe, 2016; Fig. 2). This seep was selected because it responds rapidly to rainfall. EH2 was located at a roadside outcrop in the Spray Formation (mudstone-dominant) along the west coast of the island. Seepage occurred through bedding planes in the mudstone at the base of a ~ 10–15 m slope.

Thermal infrared images were captured using a SC7650 thermal infrared camera manufactured by FLIR Systems, Inc. The camera uses an indium antimonide detector with a resolution of

Table 1
Hydraulic parameters input to the Green and Ampt equation.

K_s (mm/hr)	θ_i					θ_s	S_{av} (mm)
2.4×10^{-02}	5.0×10^{-03}	6.0×10^{-03}	7.0×10^{-03}	8.0×10^{-03}	9.0×10^{-03}	1.0×10^{-02}	$-1.0 \times 10^{+04}$

640 x 512 to measure infrared radiation in the range of 1.5–5.1 μm (FLIR, 2014). The accuracy of the camera is ± 1 °C within the standard temperature range (5 °C to 300 °C) (FLIR, 2014). Outside of this range, the camera is operational between -20 °C and 55 °C, but the accuracy may decrease (FLIR Customer Support, personal communication). During this study, the temperature was slightly cooler than 5 °C on certain days in January. Because of interference from surface runoff and rainfall, as well as the risk of damaging equipment in the rain, images were captured prior to and following the heavy rain events. The morning was identified as the ideal time to capture thermal images due to minimal influence from solar radiation.

Thermal imagery detects radiation in the infrared range of the electromagnetic spectrum (~0.7–1000 μm), which is emitted by all objects above a temperature of absolute zero (Prakash, 2000). The amount of radiation emitted depends upon the emissivity of the surface, or the ability of a material to emit radiation compared to that of a black body, as well as kinetic temperature (Prakash, 2000). Instruments are sensitive to other heat sources, such as variations in emissivity from differing geologic materials and vegetation shading, and solar radiation (Loheide and Gorelick, 2006; Roeper et al., 2014). Post-processing of thermal images was carried out using ResearchIR (FLIR, 2015). Post-processing requires specifying the emissivity, which was set to 0.96, representing distilled water (Arrasmith, 2015). This value is consistent with other studies (Robinson and Davies, 1972; Pandey et al., 2013; Vivas Becerra, 2014). The minimum and maximum temperatures, which correspond to the extremes (black and white, respectively) on the color palette, were manually assigned based on the temperature probability density function generated by the software. The purpose was to filter out the tails of the probability density function and, therefore, make the color contrast between medial temperatures more apparent. Furthermore, because the focal length of the lens (50 mm) was too long to capture entire sites in one image, sites were captured in a suit of images and subsequently stitched together using Corel PHOTO-PAINT X5.

Lastly, the area corresponding to groundwater seepage was estimated to approximate the dissipation rate and time. Because the images were captured in January (cool air temperatures), the groundwater temperature, which remains relatively constant throughout the year, was warmer than air temperature. The area corresponding to groundwater seepage was estimated visually with the aid of the temperature probability density function in ResearchIR. The probability density function was useful as it displayed a bimodal distribution with the modes corresponding to the groundwater and surrounding temperature. This methodology was similar to that used by Pfister et al. (2010) to differentiate environments in a hillslope-riparian-stream system. Pixels with a temperature above the threshold that were associated with seepage (ranging from -2.5 to 1.9 °C in individual images) were marked using an isotherm, which assigns a unique color to a specified temperature range (FLIR, 2015). (Variations in temperature may be attributed to the inaccuracy of the camera and slight changes in environmental conditions). The area over which the specified temperature was present was then calculated using the software. This area included rock and ground surfaces that were wet from seepage, but observed to dry quickly. A linear regression was fit through the data representing the daily area covered by groundwater seepage and used to forecast how long it would take seepage to cease.

2.5. Stable isotopes of Water, $\delta^{18}O$ and $\delta^{2}H$

Rainfall and seepage were sampled prior to, during, and following rain events for isotopic analysis. A rainwater collection system was installed in an open, unobstructed area on a residential property on Gabriola Island (Fig. 2). The system was active from June 2015 to March 2016. During this period, 12 rain samples were collected at approximately bi-monthly to monthly intervals, using the Real-Time Ensemble Weather Forecast to predict events (Fig. 9; UBC Earth, Ocean and Atmospheric Sciences, 2016). A local resident collected samples for isotopic analysis and measured the volume of rain that fell in each rainfall event. Because the stable isotope composition of precipitation changes throughout a storm (Clark and Fritz, 1997), samples were collected for the entire duration of the storm, resulting in a well-mixed composition. Groundwater seepage samples were collected from eight active seeps at six field sites (BW1, BW2, EH1, EH2, MG, and QQ) (Fig. 2). At the site selected to examine the seepage response to heavy rainfall (EH2), groundwater seepage was collected in November and January. Samples were collected from drips or flowing water and stored in air-tight 10 mL glass vials.

The analysis of $\delta^{18}O$ and $\delta^{2}H$ was conducted at the University of British Columbia (UBC) using a Los Gatos Research (LGR) DLT-100 liquid–water isotope analyzer and reported as per mil relative to VSMOW (error $\delta^{18}O \pm 0.2‰$; $\delta^{2}H \pm 0.8‰$ VSMOW). Each sample was analyzed in duplicate, with eight repeat analyses per sample vial with standards run every ten samples to account for instrument drift. The first four analyses were ignored to ensure that no carry over from the previous sample would affect the results. The remaining four were averaged and isotope composition determined using a calibration curve derived from the standards. Standards included Calgary snow ($\delta^{18}O$ −32.81 ‰; $\delta^{2}H$ −248.9 ‰), Fiji water ($\delta^{18}O$ −6.5 ‰; $\delta^{2}H$ −41.6 ‰) and Whistler spring water ($\delta^{18}O$ −16.2 ‰; $\delta^{2}H$ −118.5 ‰).

Monthly composite stable isotope data collected on Saturna Island (Canadian Air and Precipitation Monitoring Network Station 1017098) were used to estimate the annual and seasonal amount-averaged stable isotopic rainfall composition (Environment and Climate Change Canada, 2016; IAEA/WMO, 2016). The amount-averaged composition was calculated by weighting the annual, fall, winter, spring and summer average compositions by the amount of Saturna precipitation that fell each month. The regional groundwater stable isotopic composition, representative of groundwater on the Gulf Islands, was determined using samples collected from wells during previous studies on Saturna, Hornby, and Mayne Island (Allen, 2004; Dakin et al., 1983). All well samples were averaged to calculate the regional groundwater composition.

3. Results

3.1. Groundwater level response

Three (out of 14) provincial observation wells (Well 125, Well 281, and Well 283) had few missing data and demonstrated abrupt, well-pronounced groundwater level responses immediately

Table 2
Description of observation wells and associated weather stations selected for the analysis of the relation between groundwater level rise and rainfall.

Island	Observation well	Depth to bedrock (mbgs)	Average annual depth to water table (mbgs)	Water-bearing geological unit	Nearest weather station	Distance from well to weather station (km)	Peak correlation	Peak lag time (statistically significant lag times) (hours)
Mayne	125	0.0	0.47 ± 0.22	Sandstone, bedding contacts	Mayne Island Elementary & Junior Secondary School	0.79	0.28	8 (0–21)
Salt Spring	281	3.7	5.92 ± 0.36	Mudstone	Salt Spring Elementary School & Salt Spring Middle School	3.32	0.22	12 (0–25)
Pender	283	0.3	5.30 ± 0.96	Sandstone, fractured	Mayne Island Elementary & Junior Secondary School	4.37	0.11	9 (0–19)

following rain events. The wells are located in both sandstone and mudstone formations with the bedrock depth ranging from 0.0 to 3.7 metres below ground surface (mbgs), and the average annual water table depth ranging from 0.5 to 5.9 mbgs (Table 2). In terms of geographic location, Well 125 is situated in the centre of Mayne Island, while Wells 281 and 283 are located near the coast on Salt Spring and Pender Islands, respectively (Fig. 1).

Results of the analysis at the three wells demonstrated a peak correlation that ranged from 0.11 to 0.28 and a peak lag time that ranged from 8 to 12 h (all peak correlations are statistically significant as they exceed the 95th percent confidence interval) (Table 2). Furthermore, the correlation between rainfall amount and groundwater level was statistically significant from 0 to 21 h at Well 125, 0 to 25 h at Well 281, and 0 to 19 h at Well 283. Negative lag times where groundwater level fluctuations preceded rainfall were not considered. Of the three wells, Well 125 had the highest correlation, shortest lag time, and most distinct peak lag time (Fig. 3). Well 281 had a slightly lower correlation, the longest lag time, and a bell-shaped distribution of lag times that gradually increased, peaked, and then gradually decreased. Well 283 had the lowest correlation, but exhibited a lag time and pronounced peak similar to Well 125.

The season with the highest correlation varied by well. For example, hourly changes in groundwater level in Well 125 were most strongly correlated to rainfall amount during the summer season (Table 3). The correlations between hourly changes in groundwater level in Wells 281 and 283 and rainfall amount were lower in all four seasons compared to Well 125, but were more highly correlated to rainfall amount during the autumn and winter, respectively.

The regression analysis that yielded the highest R^2 and observable relation between rainfall amount and groundwater level rise was the manual method, followed by the method relating the daily rainfall amount to the daily groundwater level rise (method 3). However, due to the high frequency of rain events in the fall and winter, it was not possible to manually relate rises in groundwater level to individual rain events for Wells 281 and 283. The analysis for these two wells therefore compared the daily groundwater level rise to the same-day rainfall amount.

A weak relationship between groundwater level rise and rainfall amount was obtained for Wells 281 and 283 (Fig. 4). Due to this weak relationship, percentile-based analyses focusing on the relationship between groundwater level rise and rainfall intensity were not conducted.

For Well 125, which has an average water table depth of 0.47 mbgs, the relationship between groundwater level rise and all rain events (regardless of rainfall intensity) during summer is strong (R^2 = 0.94). The relationship between groundwater level rise and heavy rain is slightly less strong (R^2 = 0.91) and decreases to moderate (R^2 = 0.52) as the threshold-defining heavy rainfall intensity increases from the 50th to 90th percentile (Fig. 5). Therefore, no threshold rainfall intensity to induce a groundwater level rise was identified. These results indicate that groundwater level rise is better related to all rain events than exclusively heavy rain events during the summer season. Nevertheless, groundwater level rise is more strongly related to heavy rain than light rain (10th and 25th percentile), which showed no correlation to groundwater level rise, likely due to the large storage potential of the vadose zone at this time of the year.

3.2. Infiltration modeling

3.2.1. Rainfall intensity, infiltration rate, and ponding

Fig. 6 shows the cumulative infiltration prior to ponding and the time it takes for ponding to occur for a range of rainfall intensities under various initial moisture contents. Depending on the initial moisture content of bedrock, 6.7–33.3 mm of rain infiltrates the surface before ponding occurs for a 10th percentile rain event (average rainfall intensity = 0.06 mm/hour). Furthermore, it takes 111.1–555.6 h (4.6–23.1 days) for ponding to occur. If the soil initially has a low moisture content, the rainfall event will likely end before ponding occurs. In contrast, for a 90th percentile rain event (average rainfall intensity = 1.3 mm/hour), only 0.2–0.9 mm of rain infiltrates the surface before ponding occurs, and it only takes 0.1–0.7 h (8.8–44.1 min) for ponding to occur. If the soil is initially wet, which is probable in the late fall and winter, ponding likely occurs.

The Green and Ampt model was also used to calculate ponding times during a heavy rain event on Gabriola Island in January 2016 (Fig. 6). During this event, 42.9 mm of rain fell from January 20 at 8 pm to January 22 at 12 pm. The average rainfall intensity was 1.3 mm/hour, ranging from 0.08 to 3.5 mm/hour. During each of the first two hours of rainfall, the rain intensities were 0.6 and 1.6 mm/hour, respectively. Substituting these two values into the Green and Ampt equation (Equation 2 and 3) yields the values shown in Table 4.

If the rainfall intensity during the first hour (0.6 mm/hour) had continued steadily, it would have taken 0.6 to 3.2 h for ponding to occur. However, the initial moisture content was likely relatively high prior to this rain event, as it had rained 81.4 mm during the month of January prior to the event. Therefore, ponding likely occurred in the lower range of estimates (0.6–1.3 h), suggesting that the cumulative infiltration before ponding occurred would have been quite low (0.4–0.8 mm). Moreover, if ponding had not already occurred in the first hour, the time to ponding during the second hour (rainfall intensity = 1.6 mm/hour) would be very short (only a few minutes) and the cumulative infiltration before ponding occurred would have been very low (0.2 mm) as the initial moisture content would likely have been quite high, nearing saturation. Following ponding and the generation of infiltration excess overland flow, the infiltration rate would equal the saturated

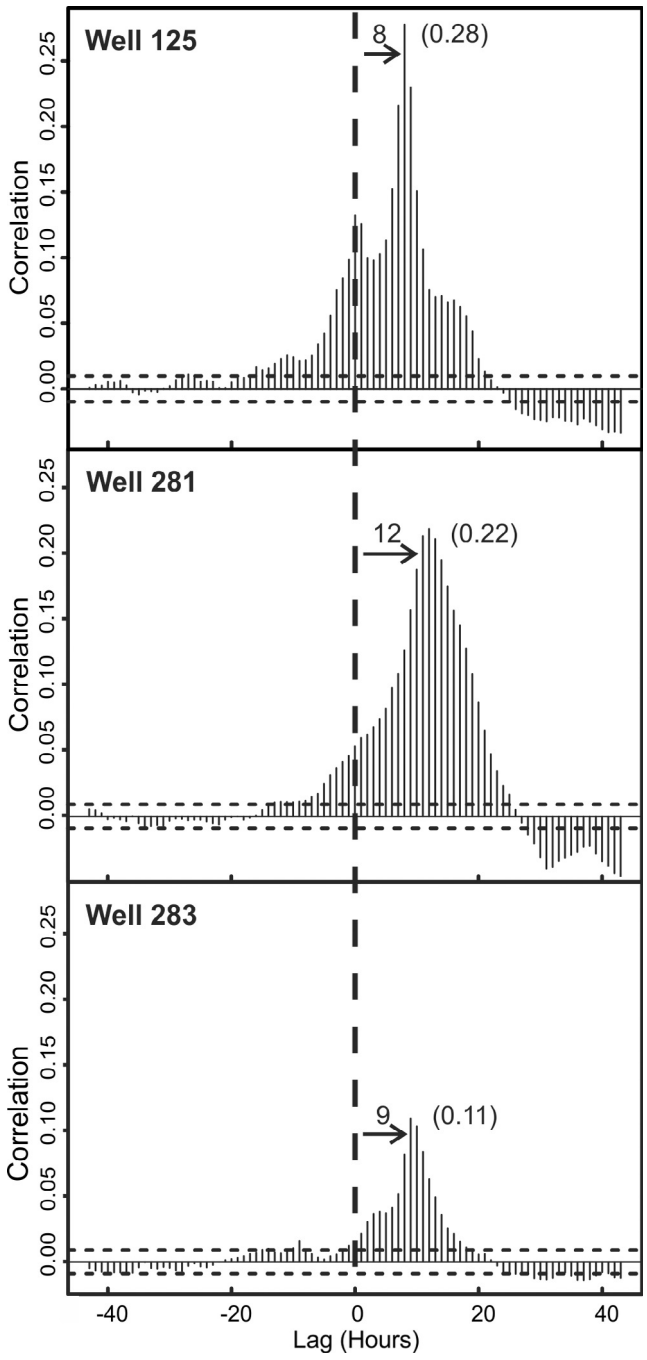

Fig. 3. Cross-correlation between rainfall amount and hourly changes in groundwater level for Wells 125, 281, and 283 from 2009 to 2015. Peak lag times are shown in parenthesis. Arrows indicate the lag time in hours. Dotted horizontal lines signify the 95% confidence interval.

Table 3
Average peak correlation by season for Wells 125, 281, and 283 from 2009-2015.

Well	Average peak correlation			
	Autumn	Winter	Spring	Summer
125	0.45	0.39	0.41	0.64
281	0.49	0.44	0.45	0.37
283	0.28	0.38	0.28	0.13

hydraulic conductivity of the bedrock (0.024 mm/hr). Infiltration would cease if the water table rose to land surface, thereby generating saturation overland flow.

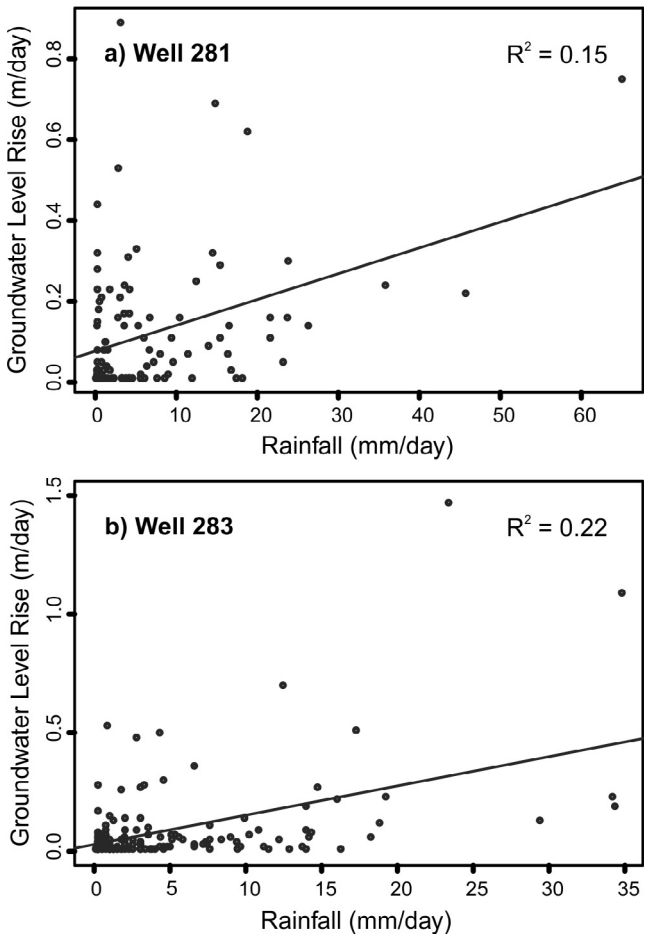

Fig. 4. Scatterplots showing the 24-h groundwater level rise versus the 24-h rainfall total at (a) Well 281 during the autumn season, and (b) Well 283 during the winter season.

3.3. Seepage characterization

The seepage response to heavy rain events in November 2015 and January 2016 was characterized for a seep at site EH2 (Fig. 2). Thermal images were captured prior to and following the heavy rain event in January 2016. Fig. 7 shows a sequence of visible light and identical thermal infrared images of the seep. Clearly evident are the bedding plane fractures that dip to the left and toward the camera. In Fig.7a, the seep is dry before rainfall. In Fig. 7b-d, seepage dissipates at roughly 24 h increments over the course of 46 h. Thus, the thermal imagery suggests a very rapid response to the rainfall event and a very rapid seepage dissipation rate at this site.

Calculation of the rate at which the seepage area dissipated (seepage area dissipation rate) suggests that seepage decreased by ~85% (from 410 cm^2 to 59 cm^2) in 46 h and likely would have ceased by ~51 h (intercept on January 24, 2016 at 1 pm) after rainfall termination (Fig. 8); this assumes that the images were captured immediately after rainfall, although there may have been some delay. Despite the well-defined seepage area dissipation rate, there is some degree of uncertainty associated with differentiating areas associated with seepage from surroundings, which limits the utility of results. Nonetheless, the seepage area dissipate rate determined from the thermal images confirms that the dissipation rate was rapid.

Fig. 9 shows the $\delta^{18}O$ composition of rain and seepage samples collected during the study, distinguishing those samples that

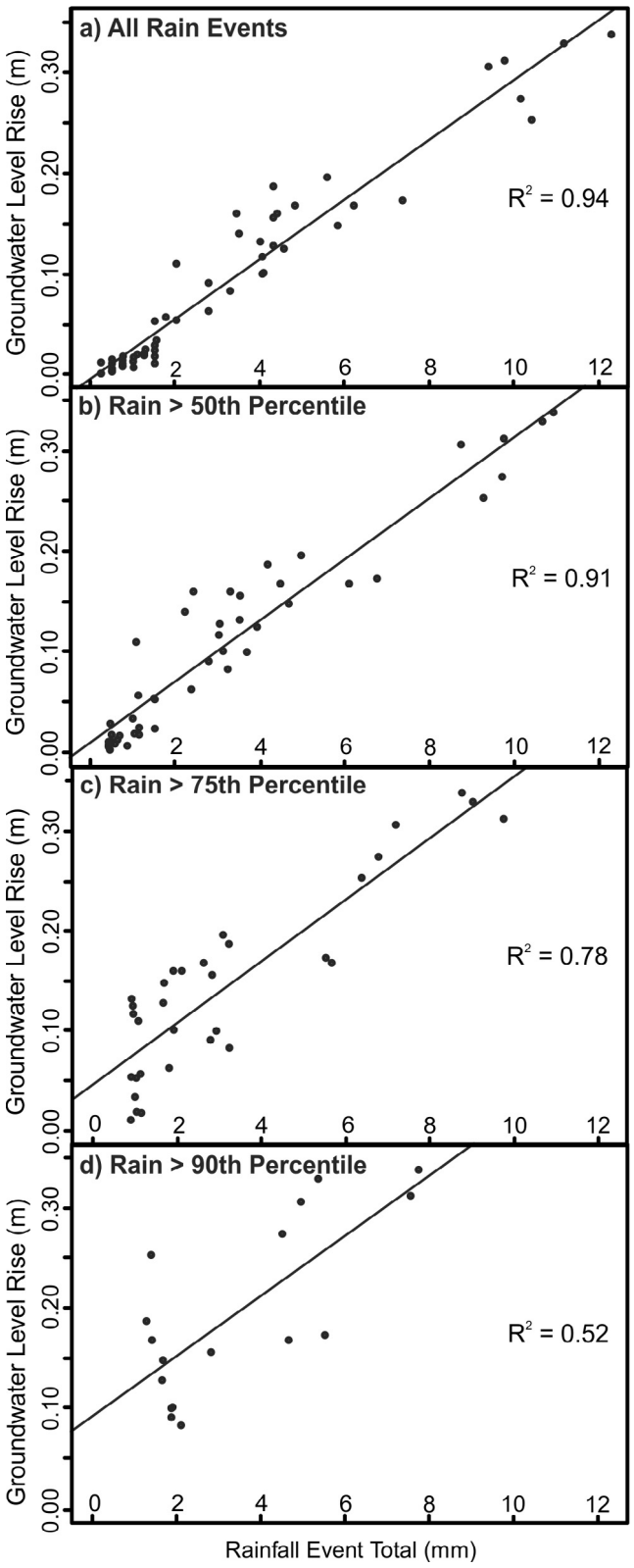

Fig. 5. Scatterplots showing groundwater level rise versus rainfall event total at Well 125 during the summer season for (a) all rain events, and rain events with intensity exceeding the (b) 50th, (c) 75th, and (d) 90th percentiles.

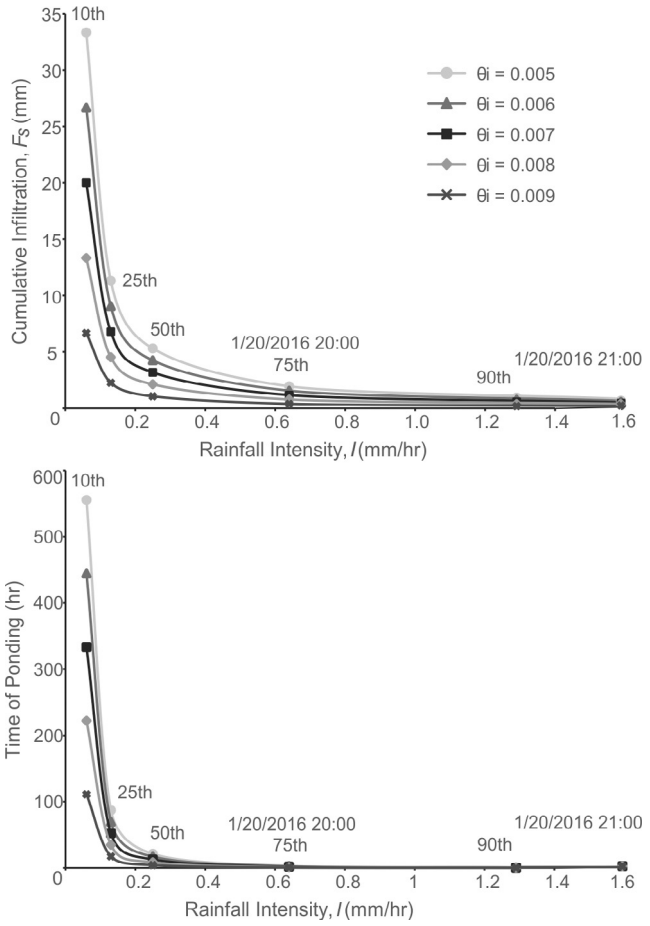

Fig. 6. Cumulative infiltration, F_s, (top) and time of ponding, t_p, (bottom) versus rainfall intensity, I, for bedrock with initial moisture content, θ_i, ranging from 0.005 to 0.009. The 10th, 25th, 50th, 75th, and 90th percentile rainfall intensities are marked, as well as the intensities during the first two hours of rainfall (1/20/2016 at 20:00 and 21:00) during a heavy rain event on Gabriola Island.

represent heavy rain events when seepage was also sampled. Also shown in Fig. 9 is the annual and seasonal amount averaged $\delta^{18}O$ composition of rainfall for Saturna Island (see Fig. 1), and the regional groundwater $\delta^{18}O$ composition representative of the Gulf Islands. The regional groundwater composition is similar to the annual amount averaged rain, as might be expected. The $\delta^{18}O$ composition of seepage collected immediately following each of two consecutive heavy rain events (separated by 28 h) in November 2015 falls between the $\delta^{18}O$ rainfall composition of the two rain events, suggesting perhaps mixing of the two rain event waters (Fig. 9). However, the seepage composition is also very similar to the autumn amount averaged rainfall composition as well as the regional groundwater composition, suggesting that the source could be autumn rainfall or groundwater. The $\delta^{18}O$ composition of seepage in January more closely resembles the $\delta^{18}O$ rainfall composition of the most recent rain event, which occurred the day of and the two days prior to seepage sampling, but it is also similar to winter rain (Fig. 9). Clearly, the January sample is not influenced by groundwater, or at least groundwater does not contribute to a significant proportion of the seepage. Rather, a recent rainfall source is indicated. This would suggest that the November samples also have recent rainfall as a source, as hydrogeological conditions at the seep location do not vary considerably from November through to late February.

4. Discussion

Fig. 10 shows conceptually that seasonal differences in the water table height set the context for the complex interactions between precipitation, recharge and the generation of overland

Table 4
Cumulative infiltration, F_s, and time of ponding, t_p, (in hours) for different rainfall intensities, I, for each of the first two hours of rain of a heavy rain event on Gabriola Island in January 2016. Initial moisture contents, θ_i, range from 0.005 to 0.009. Bold values indicate the likely time for ponding during this rain event.

Date	*I (mm/hr)*	F_s (mm)					t_p (hr)				
		θ_i = 0.005	θ_i = 0.006	θ_i = 0.007	θ_i = 0.008	θ_i = 0.009	θ_i = 0.005	θ_i = 0.006	θ_i = 0.007	θ_i = 0.008	θ_i = 0.009
1/20/2016 20:00	0.6	2.0	1.6	1.2	**0.8**	**0.4**	3.2	2.6	1.9	**1.3**	**0.6**
1/20/2016 21:00	1.6	0.8	0.6	0.5	0.3	**0.2**	0.5	0.4	0.3	0.2	**0.1**

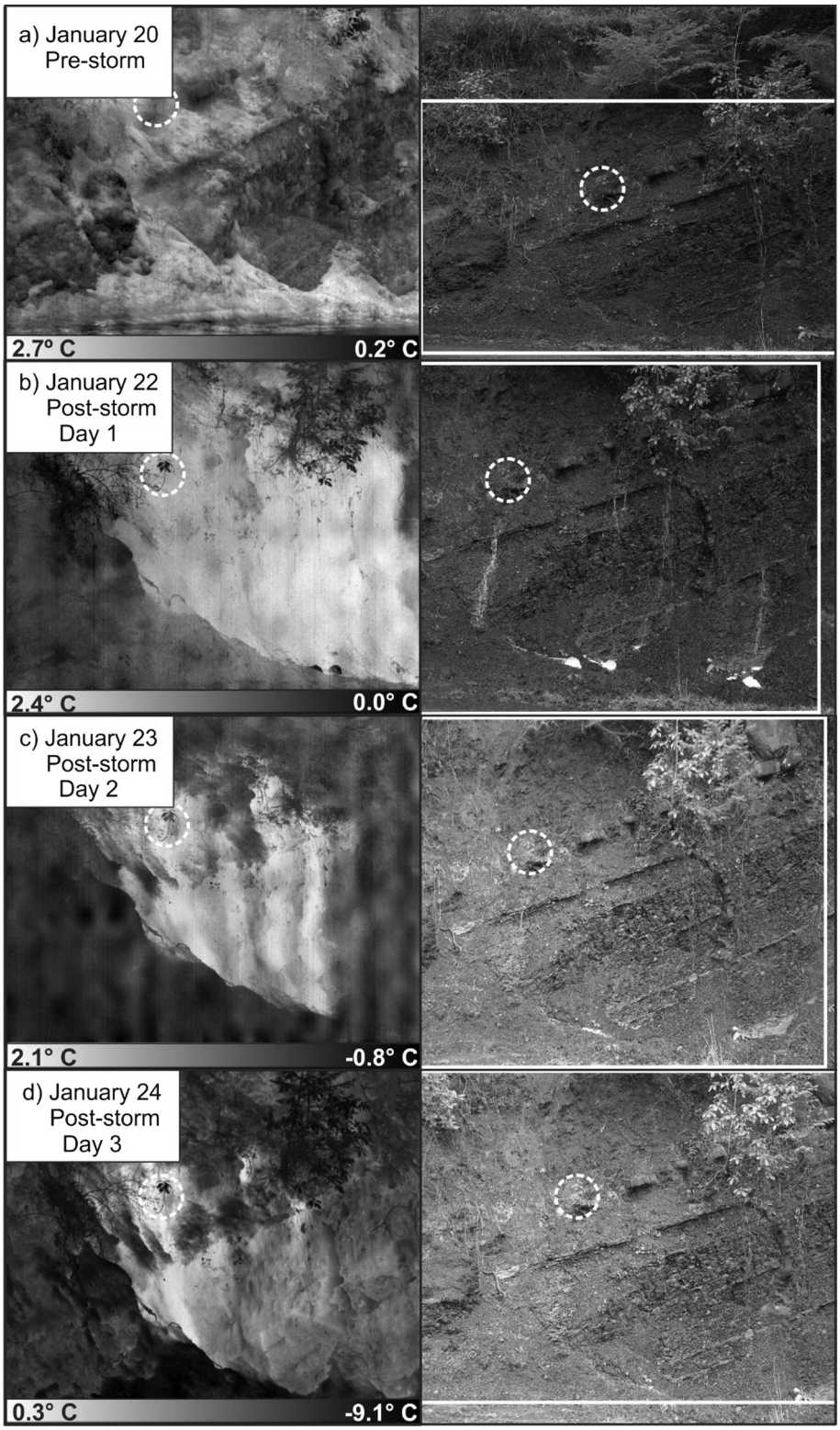

Fig. 7. Thermal images (left) showing groundwater seepage along bedding planes (a) before and (b, c, d) after a heavy rain event. The white framed visible light photos (right) correspond to the adjacent thermal image (left) with a distinct plant circled for reference.

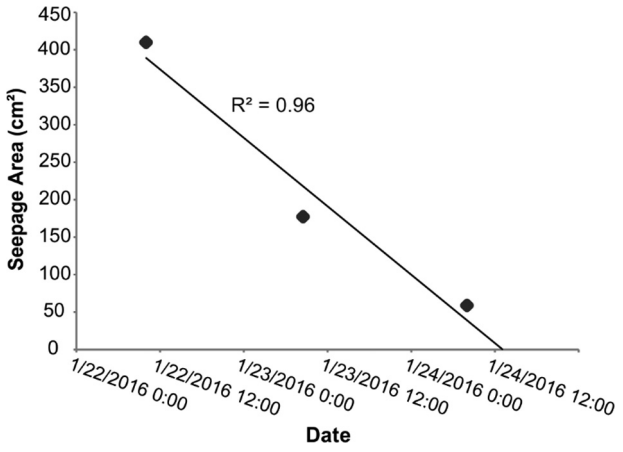

Fig. 8. Plot of the daily estimated seepage area covering EH2 from January 22, 2016 to January 24, 2016. Seepage would have ceased on January 24, 2016 at 1 pm (~51 h after rainfall termination).

flow in the temperate and mountainous Gulf Islands region. In the summer, rainfall is limited and the evapotranspiration high. The water table is generally deep, except perhaps in lower elevation areas where it may intersect or approach the land surface and form seeps. In contrast, in the winter the water table is relatively shallow. In upland areas, the water table typically remains below ground surface, while at lower elevations, particularly in depressions and along the coast, seepage is more prevalent due to the water table persistently intersecting the land surface. The bedrock is either exposed at surface or is covered by a thin veneer of soil. While the fracture permeability is relatively high, the storage capacity is generally quite limited, resulting in the fracture porosity quickly filling up. It is within this context that the results of this study are interpreted.

Despite the relatively large number of provincial groundwater observation wells (14) throughout the Gulf Islands, only three had suitably high quality datasets such that they could be analyzed statistically for relations between groundwater level response and rainfall amount. Well 125 had stronger correlations between groundwater level and rainfall amount in all seasons compared to

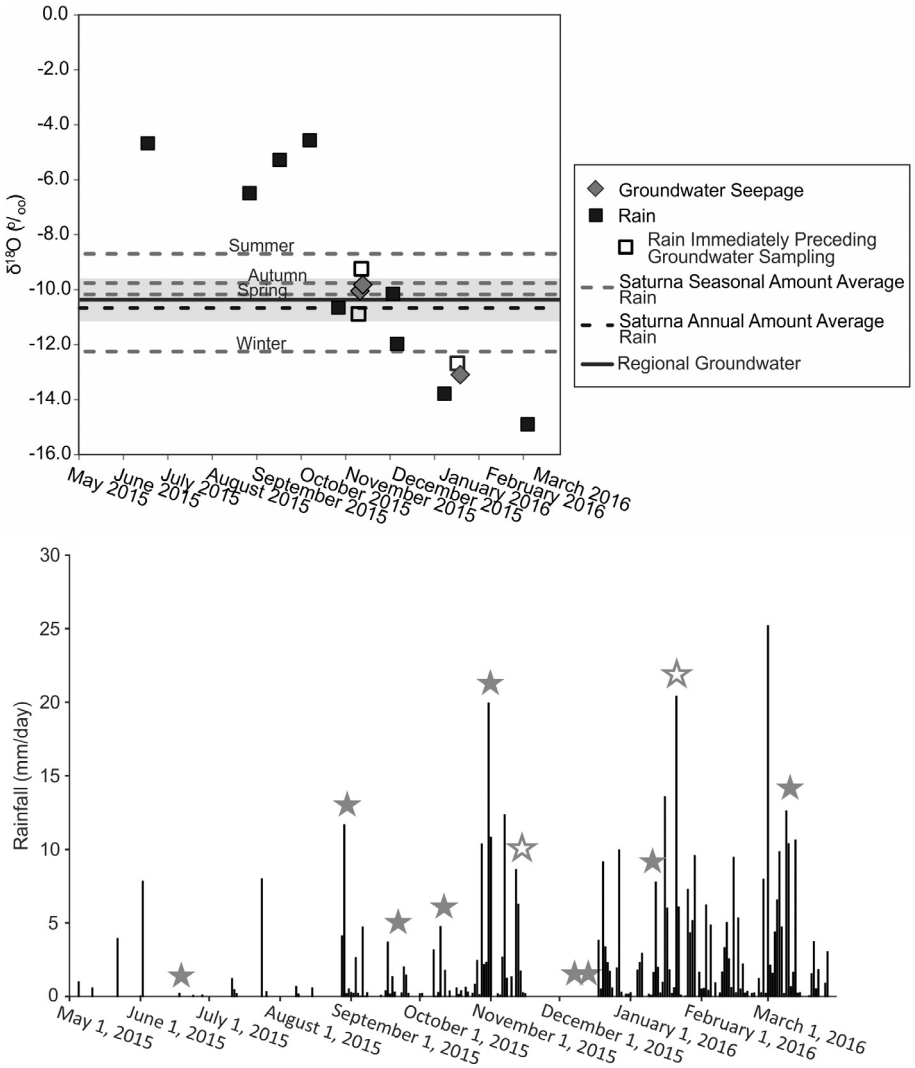

Fig. 9. The similarity in $\delta^{18}O$ composition of groundwater samples collected at EH2 and immediately preceding rainfall from May 2015 to March 2016 (top). Samples are compared against the Saturna seasonal and annual amount-averaged $\delta^{18}O$ composition of rain and the regional groundwater composition (data from Allen, 2004; Dakin et al., 1983; IAEA/WMO, 2016; Environment and Climate Change Canada, 2016). The shaded area represents one standard deviation from the mean regional groundwater composition. A rainfall chart shows daily precipitation over the same period (bottom). Solid grey stars indicate times of rainfall sampling, while hollow grey stars indicate field visits where both rainfall and groundwater seepage were sampled.

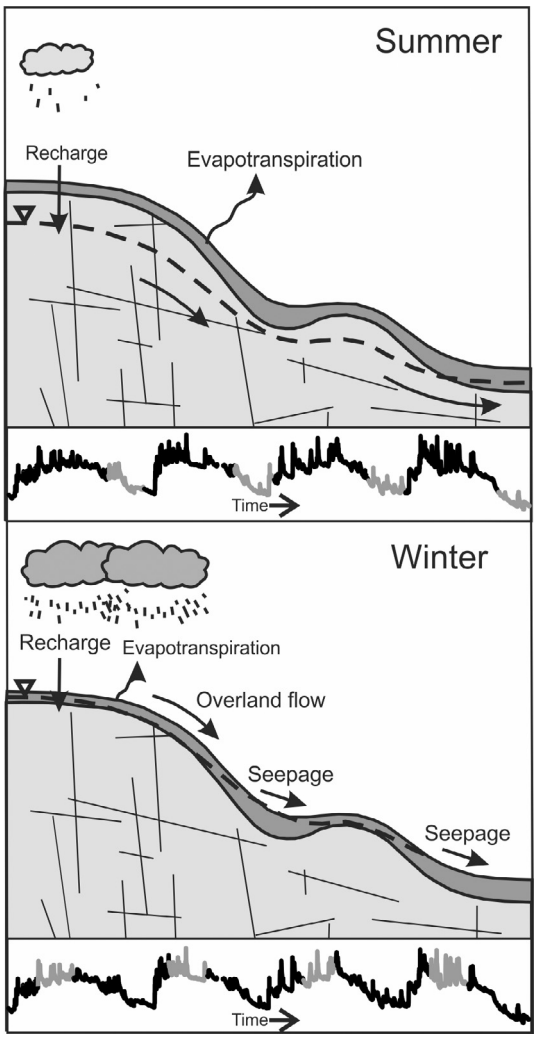

Fig. 10. Conceptualization of differences in the recharge process during the summer versus the winter. Hydrographs show the groundwater level from 2011 to 2015 in Well 125. The grey section of the hydrographs indicates the groundwater level during the summer (top) and winter (bottom).

Wells 281 and 283. The highest correlation was during the summer (0.64). During the other seasons, correlations were of similar magnitudes (0.39–0.45) to those in Well 281 (0.44–0.49). Well 283 had much lower correlations in all seasons (0.13–0.38). Differences in seasonal correlation between Well 125, and Wells 281 and 283 are likely related to the depth of the water table below ground surface. The average annual water table in Well 125 was approximately 0.47 mbgs, while it was deep (5–6 mbgs) in Wells 281 and 283. However, because Wells 281 and 283 are located near the coast, as opposed to being centrally on the island as Well 125, it is possible that the groundwater level was reflecting a groundwater discharge signal. Interestingly, all three wells had roughly the same lag time between groundwater level response and rainfall amount (8–12 h), despite Wells 281 and 283 having much deeper water tables. Because the water table in Wells 281 and 283 is deeper than in Well 125, there is more moisture storage capacity within the vadose zone. Therefore, any rainfall that is not lost to evapotranspiration will simply contribute to soil moisture. However, during the other three seasons, more rainfall and decreased evapotranspirative demands result in a more significant groundwater level response. It is noteworthy, that Well 281 has more soil overlying bedrock (3.7 m) compared to Wells 125 and 283, where the bedrock is either exposed at surface or very shallow (0–0.3 m). Thus, depth to bedrock does not appear to be an influencing factor.

Of these three, only one (Well 125) showed sufficiently strong responses to rain events to enable more detailed analysis of groundwater level response to rainfall intensity. The limited results of the regression analysis suggest that groundwater level rise in Well 125 is better related to all rain events than exclusively to heavy rain events during summer. During the summer, the distinct response in groundwater level to rain events is attributed to the infrequency of rain events, making it possible to identify discrete events. Nevertheless, there may have been short, high intensity periods of rainfall within much longer rainfall events, or back-to-back rainfall events separated by brief dry periods. If the periods of high intensity rainfall, which only lead to 2 mm "events", were situated in storms of the different duration and frequency, this would lead to different total rainfall volumes and a wide range of groundwater level rise. This might explain some of the variation in groundwater level rise for a rainfall event of about 2 mm with rainfall intensity >90th (Fig. 5d). During the winter, there were more consecutive days of rain, which interfered with correlating groundwater level rise to individual rain events.

The decrease in the relation between groundwater recharge and heavy rain observed in the summer is probably related to the greater likelihood of ponding and the subsequent generation of overland flow. If the rainfall rate is higher than the soil (or bedrock) infiltration capacity, which decreases as the moisture content increases, infiltration excess overland flow will occur (Dingman, 2002). Thus, despite high rainfall rates, the recharge rate will be limited to the saturated hydraulic conductivity. These results are supported by Kohut et al. (1984), who suggested that excess rainfall during these heavy rain periods does not necessarily recharge aquifers on the Gulf Islands due to physical limitations of the aquifer parameters (storativity and hydraulic conductivity). The water table at Well 125, however, is close to the surface throughout the year; therefore, at this particular location there is also the potential for generating saturated overland flow if the water table rises to ground surface. Given the link between shallow groundwater levels and the generation of saturated overland flow, which may accompany heavy rain events, it is reasonable that there would be a weak relation between heavy rain events and groundwater level rise in late fall and winter (the seasons with the most intense rain events) because the water table rises rapidly and becomes too shallow. During the summer, low intensity rain events of short duration (an overall small amount of rain) will likely be lost to evapotranspiration such that limited or no recharge occurs. Because the water table is deep in the summer, saturation overland flow will not likely occur. However, for high intensity summer rain events, the infiltration capacity of the soil/bedrock may be exceeded. If the rainfall event is of long duration, then following ponding, infiltration will slow to a rate equal to the saturated hydraulic conductivity. If the rainfall event is of short duration, then following ponding, there may be no further infiltration.

The Green and Ampt model seems to confirm that a smaller proportion of rain infiltrates the ground surface and contributes to recharge during heavy rain events relative to lighter rain. Although more water infiltrates in a shorter period, a larger quantity is lost to surface ponding and subsequent overland flow. Heavy rain events of long duration will lead to earlier ponding times and more overland flow, but recharge can still take place as long as the water table does not intersect the land surface. If heavy rain events are of short duration, then the rainfall event may cease before any measureable amount of recharge occurs.

These results have important implications for groundwater recharge under future climate change. In the Gulf Islands region, annual precipitation is projected to increase slightly, largely due to more fall and winter rain, while summer rainfall is projected

to decrease (Appaih-Adjei, 2006). Moreover, rainfall intensity is expected to increase, although the duration of heavy rainfall events is less certain. If fall and winter rain events become more intense, then surface ponding will occur more rapidly. This will lead to more overland flow, thereby potentially limiting recharge if the infiltration capacity is exceeded. Alternatively, if the water table is shallow, saturated overland flow may occur, stopping recharge. During summer, when the water table is deeper and not a limiting factor, recharge will likely decrease given that total summer rainfall is projected to decrease, and if either light or heavy rain events become more frequent, these would likely lead to less recharge.

Thermal infrared imagery and the $\delta^{18}O$ and $\delta^{2}H$ composition of rainfall and groundwater seepage collected in response to a heavy rain event on Gabriola Island in January 2016 point to very rapid seepage generation at this site. The $\delta^{18}O$ composition of the seepage closely approximates the composition of the immediately preceding heavy rain event, or at least seasonal rainfall. The location of seepage at site EH2 (along bedding planes that intersected the slope, not visibly near the soil–bedrock contact), suggests that seepage may have formed due to the water table rising and intersecting the land surface, generating a seepage face, or that throughflow occurred above the water table. The actual mechanism leading to the development of seepage is uncertain.

Additionally, uncertainty related to seepage characterization and analytical modeling includes:

1. Capturing thermal images when the air temperature was slightly below the standard temperature range of the camera (5 °C – 300 °C) in November and December (FLIR, 2014). This potentially reduced the camera accuracy to less than ± 1 °C.
2. Inability to control environmental conditions when thermal images were captured. For example, solar radiation is influence by solar elevation, cloud cover, atmospheric conditions (e.g., wind), etc. (Prakash, 2000). In a natural environment, it is not feasible to control all factors, although effort can be made to maintain conditions as constant as possible.
3. Collection of rain samples, which were assumed to have a well-mixed isotopic composition, representative of the entire event. During some storms, especially in the wintertime, it was difficult to differentiate one storm from another, and collect measurements precisely with the onset and termination of the storm.
4. Assumptions of the Green and Ampt model (i.e. no evapotranspiration, one-dimensional vertical infiltration, homogeneous geological material, and a uniform wetting front).
5. Complexities of modeling fractured bedrock. Infiltration to fractured bedrock is thought to be controlled by small-scale discrete fractures and may vary from the bedrock properties derived from larger scale testing methods like aquifer tests (Haught, 2010; Larocque, 2014). Moreover, values for bedrock properties were derived from studies that expressed a relatively large degree of uncertainty in hydraulic properties (Haught, 2010), or a range in reported values (Dakin et al., 1983; England, 1989; and Surrette et al., 2008). However, given the nature of fractures, a larger degree of uncertainty is often involved in estimating the properties of bedrock relative to porous media.

Future work could attempt to reproduce results with more field data (thermal infrared images and stable isotope geochemistry), or at other fractured bedrock sites in temperate regions. More observations would be useful determine whether throughflow or saturated overland flow (or both) tend to occur in response to heavy rain events. Any observations of overland flow could support the analytical findings that ponding and subsequent overland flow occurs more quickly, and is therefore more likely to occur, at higher rainfall magnitudes. Additionally, other factors could be used to characterize the seepage response, such as catchment area. Numerical modeling could also be conducted to investigate rainfall-recharge processes and climate change impacts in temperate regions. It is recommended that future modeling be conducted using a two- or three-dimensional code. This would allow for simulation of heterogeneous soil and bedrock properties and lateral flow, specifically throughflow.

5. Conclusions

The aim of this study was to contribute to our understanding of the response of fractured bedrock aquifers in temperate regions to heavy rainfall events. The study area was the Gulf Islands in British Columbia. Both the recharge and discharge environment were investigated by examining the groundwater level response to rainfall, constructing an analytical model to explore the impact of more frequent heavy rainfall events on groundwater recharge, and carrying out a field study to characterize the seepage response following heavy rainfall events.

The groundwater level response to rainfall was examined on an hourly time scale by compiling groundwater observation well and climate station records in the Gulf Islands, and conducting a regression analysis to determine if there is a threshold rainfall amount that results in a distinguishable response in groundwater level. Limited results at one observation well with a shallow aquifer and no overburden (Well 125) indicate that groundwater level rise (recharge) is more strongly correlated to all rain events than exclusively heavy rain events. The correlation gradually decreased from strong (0.94) to moderate (0.52) as different threshold-defining heavy rainfall intensities were tested, increasing from the 50th (0.42 mm/hr) to the 75th (0.87 mm/hr) to the 90th (1.25 mm/hr) percentiles. Therefore, no threshold rainfall intensity was identified. At the two other wells with deeper aquifers and overburden (Wells 281 and 283), a weak correlation was observed between groundwater level rise and rainfall (0.15 and 0.22, respectively).

The analytical model constructed to explore the impact of more frequent heavy rainfall events on groundwater recharge in the future was a modified version of the Green and Ampt model (Mein and Larson, 1973). The time of surface ponding and cumulative infiltration in exposed fractured bedrock (no surficial sediment) was calculated for various magnitude rain events (10th, 25th, 50th, 75th, and 90th percentiles). As the rainfall intensity was increased from the 10th (0.06 mm/hr) to 90th (1.3 mm/hr) percentile, surface ponding occurred sooner, resulting in less infiltration before ponding. For higher intensity rain events, more water infiltrated in a shorter period of time, but more water was also lost to surface ponding. More frequent, heavy rain events, particularly during fall and winter, projected under future climate change will likely lead to less groundwater recharge in temperate regions where the water table is shallow and the ground is wet.

A rapid seepage response to a heavy rain event in January 2016 was captured at one site using thermal infrared imagery. The seepage dissipation rate was also high. The $\delta^{18}O$ and $\delta^{2}H$ composition of the seepage, which closely resembled the isotopic composition of the heavy rain event, supported the observation that seepage occurred rapidly. Based on the stable isotope composition and location of seepage, the response was interpreted to be either throughflow or saturated overland flow (development of a seepage face).

Results of this study are primarily applicable to unconfined aquifers with shallow water tables and relatively little to no surficial sediment cover. Nonetheless, aquifers in temperate regions typically have shallow water tables. Aquifers with deeper water

tables and greater sediment thickness probably do not show the same groundwater level response observed in the regression analysis due to the attenuation of individual rain events. Moreover, the analytical model considered here represents infiltration and surface ponding for exposed bedrock. If unconsolidated surficial materials are present, the soil layer could provide a buffering influence by storing a portion of rainfall that would otherwise contribute to ponding and overland flow during heavier rain events.

This study integrated a unique combination of methods and rare hourly data resolution to examine the response of a fractured bedrock aquifer to high intensity rainfall events. Results provide useful information to determine how the occurrence of more heavy rainfall events in future could impact groundwater recharge, and changes in storage, in temperate climates.

Acknowledgments

The authors would like to acknowledge Dr. Kirsten Zickfeld and Dr. Klaus Rathfelder for their contributions. We also thank the anonymous reviewers for their useful comments. Thanks also to Pat Lapcevic, Ryan Burgess, and Glenn Jasechko for assisting with the collection of field data. This project was funded by a Discovery Grant to Diana Allen by the Natural Sciences and Engineering Research Council of Canada (NSERC).

Appendix A. Supplementary data

Supplementary data associated with this article can be found, in the online version, at http://dx.doi.org/10.1016/j.jhydrol.2017.07.042.

References

Abbott, M., Lini, A., Bierman, P., 2000. Delta O-18, delta D and H-3 measurements constrain groundwater recharge patterns in an upland fractured bedrock aquifer Vermont, USA. J. Hydrol. 228 (1–2), 101–112. http://dx.doi.org/10.1016/S0022-1694(00)00149-9.

Allen, D.M., 2004. Determining the origin of groundwater using stable isotopes of 18O, 2H, and 34S. Ground Water 42 (1), 17–31.

Allen, M., Ingram, W., 2002. Constraints on future changes in climate and the hydrologic cycle. Nature 419 (6903), 224–232. http://dx.doi.org/10.1038/nature01092.

Allen, D., Suchy, M., 2001. Geochemical evolution of groundwater on Saturna Island British Columbia. Can. J. Earth Sci. 38 (7), 1059–1080. http://dx.doi.org/10.1139/e01-007.

Allocca, V., De Vita, P., Manna, F., Nimmo, J.R., 2015. Groundwater recharge assessment at local and episodic scale in a soil mantled perched karst aquifer in southern Italy. J. Hydrol. 529, 843–853.

Anderson, M., 2005. Heat as a ground water tracer. Ground Water 43 (6), 951–968. http://dx.doi.org/10.1111/j.1745-6584.2005.00052.x.

Appaih-Adjei, E.K., 2006. Climate Change Impacts on Groundwater Recharge in Gulf Islands, Canada (Masters thesis). Lund University, Lund Sweden.

Arrasmith, W., 2015. Systems engineering and analysis of electro-optical and infrared systems. CRC Press, Boca Raton, FL.

Banks, W., Paylor, R., Hughes, W., 1996. Using thermal-infrared imagery to delineate ground-water discharge. Ground Water 34 (3), 434–443. http://dx.doi.org/10.1111/j.1745-6584.1996.tb02024.x.

BC Ministry of Environment (2015), BC Groundwater Observation Well Network, retrieved from http://www.env.gov.bc.ca/wsd/data_searches/obswell/map/obsWells.html (November, 2015).

Bouwer, H., 1969. Infiltration of water into non-uniform soil. J. Irrig. Drain. Div. ASCE 95, 451–462.

Burgess, R., 2017. Characterizing Recharge to Fractured Bedrock in a Temperate Climate (Masters thesis). Simon Fraser University, Burnaby Canada.

Carretero, S.C., Kruse, E.E., 2012. Relationship between precipitation and water-table fluctuation in a coastal dune aquifer: Northeastern coast of the Buenos Aires Province Argentina. Hydrogeol. J. 20 (8), 1613–1621. http://dx.doi.org/10.1007/s10040-012-0890-y.

Chu, S., 1978. Infiltration during an unsteady rain. Water Resour. Res. 14 (3), 461–466. http://dx.doi.org/10.1029/WR014i003p00461.

Clague, J.J., 1986. The Quaternary stratigraphic record of British Columbia – evidence for episodic sedimentation and erosion controlled by glaciation. Can. J. Earth Sci. 23, 885–894.

Clark, I.D., Fritz, P., 1997. Environmental Isotopes in Hydrogeology. Lewis Publishers, Boca Raton, FL.

Crosbie, R.S., Jolly, I.D., Leaney, F.W., Petheram, C., 2010. Can the dataset of field based recharge estimates in Australia be used to predict recharge in data-poor areas? Hydrol. Earth Syst. Sci. 14, 2023–2038.

Cuthbert, M.O., 2010. An improved time series approach for estimating groundwater recharge from groundwater level fluctuations. Water Resour. Res. 46, W09515. http://dx.doi.org/10.1029/2009WR008572.

Dakin, R., Farvolden, R., Cherry, J., Fritz, P., 1983. Origin of dissolved solids in groundwaters of Mayne Island British-Columbia Canada. J. Hydrol. 63 (3–4), 233–270. http://dx.doi.org/10.1016/0022-1694(83)90044-6.

De Vries, J.J., Simmers, I., 2002. Groundwater recharge: an overview of processes and challenges. Hydrogeol. J. 10, 5–17.

Deitchman, R.S., Loheide II., S.P., 2009. Ground-based thermal imaging of groundwater flow processes at the seepage face. Geophys. Res. Lett. 36, L14401. http://dx.doi.org/10.1029/2009GL038103.

DHI (2007), MIKE SHE user manual, Volume 2: Reference Guide, Danish Hydraulic Institute: Denmark.

Dingman, S.L., 2002. Physical Hydrology. Prentice Hall, Upper Saddle River, New Jersey.

Dvory, N.Z., Livshitz, Y., Kuznetsov, M., Adar, E., Yakirevich, A., 2016. The effect of hydrogeological conditions on variability and dynamic of groundwater recharge in a carbonate aquifer at local scale. J. Hydrol. 535, 480–494.

England, T. D. J. (1989), Late Cretaceous to Paleogene evolution of the Georgia Basin, Southwestern British Columbia, Ph.D. thesis, Memorial University of Newfoundland, St. John's, Canada.

Environment Canada (2016), Station Results – 1981-2010 Climate Normals and Averages, retrieved from http://climate.weather.gc.ca/climate_normals/results_1981_2010_e.html?stnID=172&radius=25&proxSearchType=coordinates&degreesNorth=49&minutesNorth=11&secondsNorth= 56&degreesWest=123&minutesWest=59&secondsWest=16&proxSubmit=go&dCode=0 (October, 2016).

Environment and Climate Change Canada (2016), Historical Data – Saturna CAPMoN, retrieved from http://climate.weather.gc.ca/climate_data/monthly_data_e.html?hlyRange=%7C&dlyRange=1989-06-01%7C2015-06-30&mlyRange=1989-01-01%7C2007-02-01&StationID=95&Prov=BC&urlExtension=_e.html&searchType=stnName&optLimit=yearRange&StartYear=1997&EndYear=2010&selRowPerPage=25&Line=0&searchMethod=contains&Month=7&Day=9&txtStationName=saturna&timeframe=3&Year=2007 (August, 2016).

FLIR Systems, Inc. (2014), FLIR SC7000 Datasheet, retrieved from http://www.flirmedia.com/MMC/THG/Brochures/RND_017/RND_017_US.pdf (July, 2016).

FLIR Systems, Inc. (2015), ResearchIR 4: User's Guide, retrieved from http://assets.techedu.com/assets/1/26/FLIR_ResearchIR_User_Manual1.pdf (July 2016).

Gburek, W., Folmar, G., 1999. A ground water recharge field study: site characterization and initial results. Hydrol. Process. 13 (17), 2813–2831. http://dx.doi.org/10.1002/(SICI)1099-1085(19991215)13:17<2813::AID-HYP901>3.3.CO;2-Y.

Gleeson, T., Novakowski, K., Kyser, T.K., 2009. Extremely rapid and localized recharge to a fractured rock aquifer. J. Hydrol. 376 (3–4), 496–509. http://dx.doi.org/10.1016/j.jhydrol.2009.07.056.

Green, W.H., Ampt, G., 1911. Studies of soil physics, part 1: the flow of air and water through soils. J. Agric. Soc. 4, 1–24.

Green, T.R., Taniguchi, M., Kooi, H., Gurdak, J.J., Allen, D.M., Hiscock, K.M., Treidel, H., Aureli, A., 2011. Beneath the surface of global change: impacts of climate change on groundwater. J. Hydrol. 405 (3–4), 532–560. http://dx.doi.org/10.1016/j.jhydrol.2011.05.002.

Hare, D.K., Briggs, M.A., Rosenberry, D.O., Boutt, D.F., Lane, J.W., 2015. A comparison of thermal infrared to fiber-optic distributed temperature sensing for evaluation of groundwater discharge to surface water. J. Hydrol. 530, 153–166. http://dx.doi.org/10.1016/j.jhydrol.2015.09.059.

Haught, D. (2010), Runoff generation mechanisms in a steep first-order British Columbian watershed, M.Sc. thesis, Simon Fraser University, Burnaby, Canada.

Healy, R.W., Cook, P.G., 2002. Using groundwater levels to estimate recharge. Hydrogeol. J. 10 (1), 91–109. http://dx.doi.org/10.1007/s10040-001-0178-0.

Healy, R.W., B.R. Scanlon (2010), Estimating groundwater recharge: Cambridge University Press, New York, NY.

Heppner, C.S., Nimmo, J.R., Folmar, G.J., Gburek, W.J., Risser, D.W., 2007. Multiple-methods investigation of recharge at a humid-region fractured rock site, Pennsylvania, USA. Hydrogeol. J. 15 (5), 915–927. http://dx.doi.org/10.1007/s10040-006-0149-6.

Horton, R.E., 1940. An approach towards physical interpretation of infiltration capacity. Proc. Soil Sci. Soc. Am. 5, 399–417.

IAEA/WMO (2016), Global network of isotopes in precipitation, The GNIP database, retrieved from http://www.iaea.org/water (July, 2016).

Intergovernmental Panel on Climate Change (IPCC) (2012), Managing the Risks of Extreme Events and Disasters to Advance Climate Change Adaptation, Field, C. B., Barros, V., Stocker, T. F., Qin, D., Dokken, D. J., Ebi, K. L., Mastrandrea, M. D., Mach, K. J., Plattner, G.-K., Allen, S. K., Tignor, M., and P. M. Midgley, Cambridge University Press, Cambridge, UK, and New York, NY, USA, pp. 1-19, retrieved from http://ipcc-wg2.gov/SREX/ (February, 2015).

Islands Trust (2009), Gabriola Island Community Profile, retrieved from http://www.islandstrust.bc.ca/ltc/gb/pdf/gbrptcommunityprofile.pdf (December, 2015).

James, W., Warinner, J., Reedy, M., 1992. Application of the Green-Ampt infiltration equation to watershed modeling. Water Resour. Bull. 28 (3), 623–635.

Jyrkama, M.I., Sykes, J.F., 2007. The impact of climate change on spatially varying groundwater recharge in the Grand River watershed (Ontario). J. Hydrol. 338 (3–4), 237–250. http://dx.doi.org/10.1016/j.jhydrol.2007.02.036.

Katsuyama, M., Ohte, N., Kabeya, N., 2005. Effects of bedrock permeability on hillslope and riparian groundwater dynamics in a weathered granite catchment. Water Resour. Res. 41 (1), W01010. http://dx.doi.org/10.1029/2004WR003275.

Kohut, A.P., Hodge, W.S., Johanson, D.A., Kalyn, D., 1984. Natural seasonal response of groundwater levels in fractured bedrock aquifers of the Southern Coastal Region of British Columbia. International Groundwater Symposium on Groundwater Resources Utilization and Contaminant Hydrogeology, International Association of Hydrogeologists, Canadian National Chapter.

Larocque, I. (2014), The Hydrogeology of Salt Spring Island, British Columbia, M.Sc. thesis, Simon Fraser University, Burnaby, Canada.

Lee, K., Wenner, D., Lee, I., 1999. Using H- and O-isotopic data for estimating the relative contributions of rainy and dry season precipitation to groundwater: example from Cheju Island Korea. J. Hydrol. 222 (1–4), 65–74. http://dx.doi.org/10.1016/S0022-1694(99)00099-2.

Loheide II, S.P., Gorelick, S.M., 2006. Quantifying stream-aquifer interactions through the analysis of remotely sensed thermographic profiles and in situ temperature histories. Environ. Sci. Technol. 40 (10), 3336–3341. http://dx.doi.org/10.1021/es0522074.

Mackie, D. C. (2002), An integrated structural and hydrogeologic investigation of the fracture system in the upper Cretaceous Nanaimo Group, southern Gulf Islands, British Columbia, M.Sc. thesis, Simon Fraser University, Burnaby, Canada.

Mein, R.G., Larson, C.L., 1971. Modeling of the Infiltration Component of the Rainfall-runoff Process, Bulletin 43, 21–29. University of Minnesota, Minneapolis, Water Resources Research Center.

Mein, R., Larson, C., 1973. Modeling infiltration during a steady rain. Water Resour. Res. 9 (2), 384–394. http://dx.doi.org/10.1029/WR009i002p00384.

Mileham, L., Taylor, R.G., Todd, M., Tindimugaya, C., Thompson, J., 2009. The impact of climate change on groundwater recharge and runoff in a humid, equatorial catchment: sensitivity of projections to rainfall intensity. Hydrol. Sci. J. 54 (4), 727–738. http://dx.doi.org/10.1623/hysj.54.4.727.

Mustard, P.S., 1994. The upper Cretaceous Nanaimo Group Georgia Basin, Geology and geological hazard of the Vancouver region, southwestern British Columbia. Bulletin 481, 27–95.

Nimmo, J.R., Horowitz, C., Mitchell, L., 2015. Discrete-storm water-table fluctuation method to estimate episodic recharge. Groundwater 53, 282–292.

Owor, M., Taylor, R.G., Tindimugaya, C., Mwesigwa, D., 2009. Rainfall intensity and groundwater recharge: Empirical evidence from the upper Nile basin. Environ. Res. Lett. 4 (3), 035009. http://dx.doi.org/10.1088/1748-9326/4/3/035009.

Pall, P., Allen, M.R., Stone, D.A., 2007. Testing the Clausius-Clapeyron constraint on changes in extreme precipitation under CO2 warming. Clim. Dyn. 28 (4), 351–363. http://dx.doi.org/10.1007/s00382-006-0180-2.

Pandey, P., Gleeson, T., Baraer, M., 2013. Toward quantifying discrete groundwater discharge from frozen seepage faces using thermal infrared images. Geophys. Res. Lett. 40 (1), 123–127. http://dx.doi.org/10.1029/2012GL054315.

Pfister, L., McDonnell, J.J., Hissler, C., Hoffmann, L., 2010. Ground-based thermal imagery as a simple, practical tool for mapping saturated area connectivity and dynamics. Hydrol. Process. 24 (21), 3123–3132. http://dx.doi.org/10.1002/hyp.7840.

Philip, J.R., 1957. The Theory of Infiltration, 1: the infiltration equation and its solution. Soil Sci. 83 (5), 345–357.

Praamsma, T., Novakowski, K., Kyser, K., Hall, K., 2009. Using stable isotopes and hydraulic head data to investigate groundwater recharge and discharge in a fractured rock aquifer. J. Hydrol. 366 (1–4), 35–45. http://dx.doi.org/10.1016/j.jhydrol.2008.12.011.

Prakash, A. (2000), Thermal remote sensing: Concepts, issues, and applications, International Archives of Photogrammetry and Remote Sensing, Vol. XXXIII, Part B1, 239-243, Amsterdam, retrieved from http://www.isprs.org/proceedings/XXXIII/congress/part1/239_XXXIII-part1.pdf (March, 2015).

Robinson, P., Davies, J., 1972. Laboratory determinations of water surface emissivity. J. Appl. Meteorol. 11 (8), 1391–1393. http://dx.doi.org/10.1175/1520-0450(1972)011<1391:LDOWSE>2.0.CO;2.

Roeper, T., Greskowiak, J., Massmann, G., 2014. Detecting small groundwater discharge springs using handheld thermal infrared imagery. Groundwater 52 (6), 936–942. http://dx.doi.org/10.1111/gwat.12145.

RStudio Team, 2015. RStudio: Integrated development for R. RStudio Inc, Boston, MA, Version (99), 486.

Salve, R., Ghezzehei, T.A., Jones, R., 2008. Infiltration into fractured bedrock. Water Resour. Res. 44 (1), W01434. http://dx.doi.org/10.1029/2006WR005701.

Scanlon, B., Healy, R., Cook, P., 2002. Choosing appropriate techniques for quantifying groundwater recharge. Hydrogeol. J. 10 (1), 18–39. http://dx.doi.org/10.1007/s10040-001-0176-2.

Schuetz, T., Weiler, M., 2011. Quantification of localized groundwater inflow into streams using ground-based infrared thermography. Geophys. Res. Lett. 38, L03401. http://dx.doi.org/10.1029/2010GL046198.

Scibek, J., Allen, D.M., 2006. Modeled impacts of predicted climate change on recharge and groundwater levels. Water Resour. Res. 42 (11), W11405. http://dx.doi.org/10.1029/2005WR004742.

Scibek, J., Mackie, D., Sivak, T., Petersmeyer, C.W., 2013. Regional district of Nanaimo Water Budget Project, Gabriola, DeCourcy, and Mudge Islands – Phase 1: hydrogeological conceptual model and water budget. SRK Consulting & Thurber Engineering Ltd., Submitted to Regional District of Nanaimo.

Statistics Canada (2015), Population and dwelling counts for Canada, provinces and territories, and designated places, 2011 and 2006 censuses, retrieved from http://www12.statcan.ca/census-recensement/2011/dp-pd/hlt-fst/pd-pl/Table-Tableau.cfm?LANG=Eng&T=1302&SR=101&S=51&O=A&RPP=25&PR=59&CMA=0 (December, 2015).

Surrette, M., Allen, D.M., 2008. Quantifying heterogeneity in fractured sedimentary rock using a hydrostructural domain approach. Geol. Soc. Am. Bull. 120 (1), 225–237.

Surrette, M., Allen, D.M., Journeay, M., 2008. Regional evaluation of hydraulic properties in variably fractured rock using a hydrostructural domain approach. Hydrogeol. J. 16 (1), 11–30. http://dx.doi.org/10.1007/s10040-007-0206-9.

Taylor, R.G., Todd, M.C., Kongola, L., Maurice, L., Nahozya, E., Sanga, H., MacDonald, A.M., 2013. Evidence of the dependence of groundwater resources on extreme rainfall in East Africa. Nat. Clim. Change 3 (4), 374–378. http://dx.doi.org/10.1038/NCLIMATE1731.

Toews, M.W., Allen, D.M., 2009. Simulated response of groundwater to predicted recharge in a semi-arid region using a scenario of modelled climate change. Environ. Res. Lett. 4 (3), 035003. http://dx.doi.org/10.1088/1748-9326/4/3/035003.

Tromp-van Meerveld, H.J., Peters, N.E., McDonnell, J.J., 2007. Effect of bedrock permeability on subsurface stormflow and the water balance of a trenched hillslope at the Panola Mountain Research Watershed, Georgia, USA. Hydrol. Processes 21 (6), 750–769. http://dx.doi.org/10.1002/hyp.6265.

Turkeltaub, T., Kurtzman, D., Bel, G., Dahan, O., 2015. Examination of groundwater recharge with a calibrated/validated flow model of the deep vadose zone. J. Hydrol. 522, 618–627. http://dx.doi.org/10.1016/j.jhydrol.2015.01.026.

University of British Columbia Earth, Ocean and Atmospheric Sciences - Weather Forecast Research Team (2016), Real-time Ensemble Weather Forecast for Western Canada, retrieved from http://weather.eos.ubc.ca/wxfcst/ (August, 2016).

Vivas Becerra, J. (2014), Groundwater characterization and modeling in natural and open pit rock slopes, M.Sc. thesis, Simon Fraser University, Vancouver, Canada.

Walter, T. (2011), Green and Ampt Infiltration [Class handout], Physical Hydrology for Ecosystems, Department of Biological and Environmental Engineering, Cornell University, Ithaca, NY, Microsoft Word file.

Weaver, A. J., and E. C. Wiebe (n.d.), Anatomy of the Weather Station, School-Based Weather Station Network, retrieved from http://www.victoriaweather.ca/anatomy.php (December, 2015).

Weaver, A. J., and E. C. Wiebe (2012a), About the School-Based Weather Station Network, School-Based Weather Station Network, retrieved from http://www.victoriaweather.ca/about.php (December, 2015).

Weaver, A. J., and E. C. Wiebe (2012b), How we installed the Weather Stations, School-Based Weather Station Network, retrieved from http://www.victoriaweather.ca/installphotos.php (December, 2015).

Weaver, A. J. and E. C. Wiebe (2015), Status of all Stations, School-Based Weather Station Network, retrieved from http://www.victoriaweather.ca/all_current_data.php (December, 2015).

Weaver, A. J., and E. C. Wiebe (2016), Station Average Data Browser – Rain total, School-Based Weather Station Network, retrieved from http://www.islandweather.ca/dataavgs.php?field=raintotal&interval=60&id=113 (October, 2016).